

Validation of the Bond et al. (2010) SDSS-derived kinematic models for the Milky Way's disk and halo stars with Gaia Data Release 3 proper motion and radial velocity data

BRUNO DOMÍNGUEZ,¹ SIDDHARTH CHAINI,² KARLO MRAKOVČIĆ,³ BRANDON SALLEE,⁴ AND ŽELJKO IVEZIĆ⁵

¹Departamento de Astronomía, Facultad de Ciencias, Universidad de la Repùblica, Iguá 4225, 11400, Montevideo, Uruguay

²Department of Physics and Astronomy, University of Delaware, Newark, DE 19716, USA

³Faculty of Physics, University of Rijeka, Radmila Matejčić 2, 51000 Rijeka, Croatia

⁴Department of Astronomy, University of Washington, Box 351580, Seattle, WA 98195, USA

⁵Department of Astronomy and the DiRAC Institute, University of Washington, 3910 15th Avenue NE, Seattle, WA 98195, USA;
corresponding author: ivezic@uw.edu

(Received January 3, 2024; Revised XXX; Accepted XXX)

Submitted to AJ

Abstract

We validate the Bond et al. (2010) kinematic models for the Milky Way's disk and halo stars with Gaia Data Release 3 data. Bond et al. used stellar radial velocities measured by the Sloan Digital Sky Survey (SDSS), and stellar proper motions derived from SDSS and the Palomar Observatory Sky Survey astrometric measurements, to construct models for stellar velocity distributions. Their models describe velocity distributions as functions of position in the Galaxy, and separately for disk and halo stars that were labeled using SDSS photometric and spectroscopic metallicity measurements. We find that the Bond et al. model predictions are in good agreement with recent measurements of stellar radial velocities and proper motions by the Gaia survey. In particular, the skewed non-Gaussian distribution of rotational velocity for disk stars and its vertical gradient is confirmed, and dispersions for all three velocity components are correctly predicted. The spatial invariance of velocity ellipsoid for halo stars when expressed in spherical coordinates is also confirmed by Gaia data at galacto-centric radial distances of up to 15 kpc.

Keywords: Milky Way galaxy — stellar kinematics

1. INTRODUCTION

The Milky Way is a complex and dynamic structure that is constantly being shaped by the infall of matter from the Local Group and mergers with neighboring galaxies. The advent of modern sky surveys has resulted in a wealth of data for large number of individual stars that can be used to describe and model their distribution in a nine-dimensional space spanned by the three spatial coordinates, three velocity components, and three principal stellar parameters – luminosity, effective temperature, and metallicity (for a detailed discussion and references see, e.g., Ivezić et al. 2012). The modeling of observed multi-dimensional distributions can provide in-situ constraints on the formation and evolutionary processes of a spiral galaxy, the Milky Way. For example, stellar number density and kinematic measurements, aided by models, can be used to constrain the Milky Way's dark matter distribution (e.g., Loebman et al. 2012, 2014).

Stellar distribution models are also valuable for predicting stellar content and its behavior expected in upcoming surveys, such as Rubin's Legacy Survey of Space and Time (LSST; Ivezić et al. 2019). For example, Dal Tio et al. (2022) have recently produced a massive simulated stellar catalog¹ corresponding to anticipated LSST's sky coverage and depth ($r \sim 27$). In addition to its current use in quantitative forecasting of LSST science outcome, such catalogs will become even more important as input to tools for quantifying various LSST selection functions (e.g., photometric selection of quasars, where stars are rejected using color and proper motion cuts) and for providing Bayesian priors for

¹ This catalog is publicly available from NOIRLab's Astro Data Lab portal.

science analysis (e.g., for stellar photometric distance estimation). Validation of kinematic models that can be used when generating such catalogs is the primary objective of this paper.

Bond et al. (2010) studied Milky Way kinematics using a sample of about 19 million main-sequence stars with Sloan Digital Sky Survey (SDSS) photometry and proper-motion measurements derived from the SDSS and the Palomar Observatory Sky Survey (POSS) astrometry, including a subset of $\sim 170,000$ stars with radial-velocity measurements from the SDSS spectroscopic survey. They developed a simple descriptive model for the overall kinematic behavior that captures these features over most of the probed volume (summarized in §2.1), with distances in the range from 100 pc to 10 kpc and over a quarter of the sky at high Galactic latitudes ($|b| > 20^\circ$).

Gaia's recently published photometric, radial velocity and proper motion measurements (Gaia Collaboration et al. 2021) can be used to critically assess the accuracy of Bond et al. (2010) kinematic models because of their superior uncertainties (for a comparison of SDSS and SDSS-POSS measurement uncertainties with Gaia's, see Figure 21 in Ivezić et al. 2012). In addition, with Gaia's data the model validity can be extended to distances below 100 pc (due to SDSS image saturation at $r \sim 14$), and to the four times larger full-sky area. In §2 we describe our datasets and analysis methodology, and in §3 we present our analysis results. Our main results are summarized and discussed in §4. All our results from this paper can be reproduced from our accompanying GitHub repository.²

2. DATA DESCRIPTION AND ANALYSIS METHODOLOGY

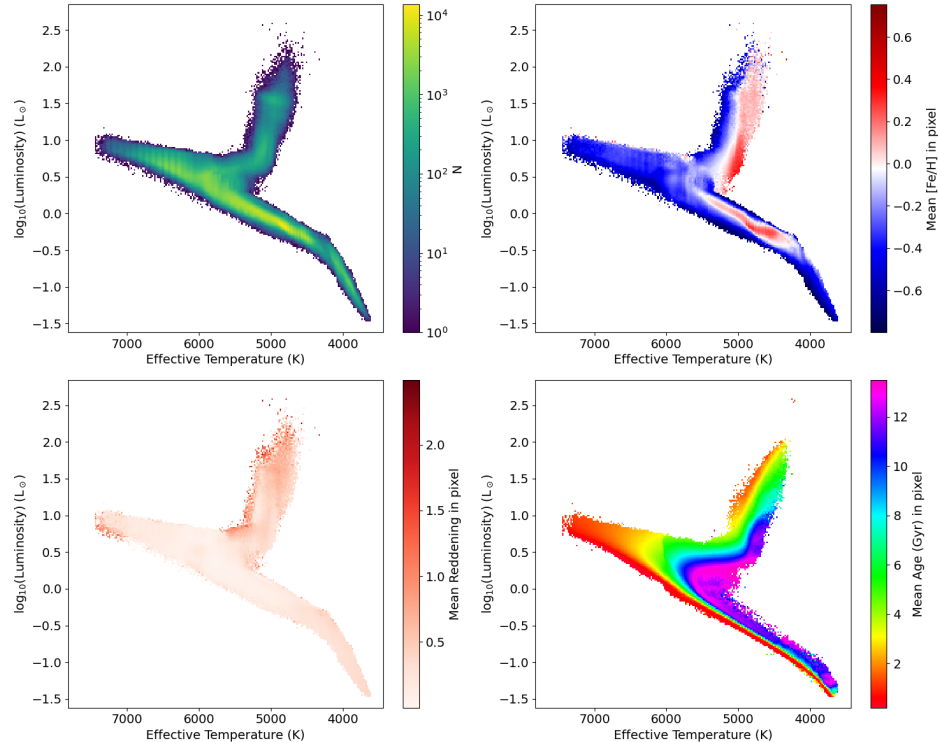


Figure 1. The distribution of 3.3 million FGKM stars discussed here in the Hertzsprung-Russell diagram. The top left panel shows stellar counts on a log scale and the remaining panels show mean per-pixel values of metallicity, interstellar dust reddening and age. Note that the hottest stars in the sample (effective temperature above 6,500 K) are also the youngest (ages below 2 Gyr).

The blue main sequence stars close to the turn-off point represent a good population for studying bulk kinematic properties in the Milky Way because they are numerous, have comparatively large limiting distances due to high

² <https://github.com/sidchaini/MWKinematicsFGKM>

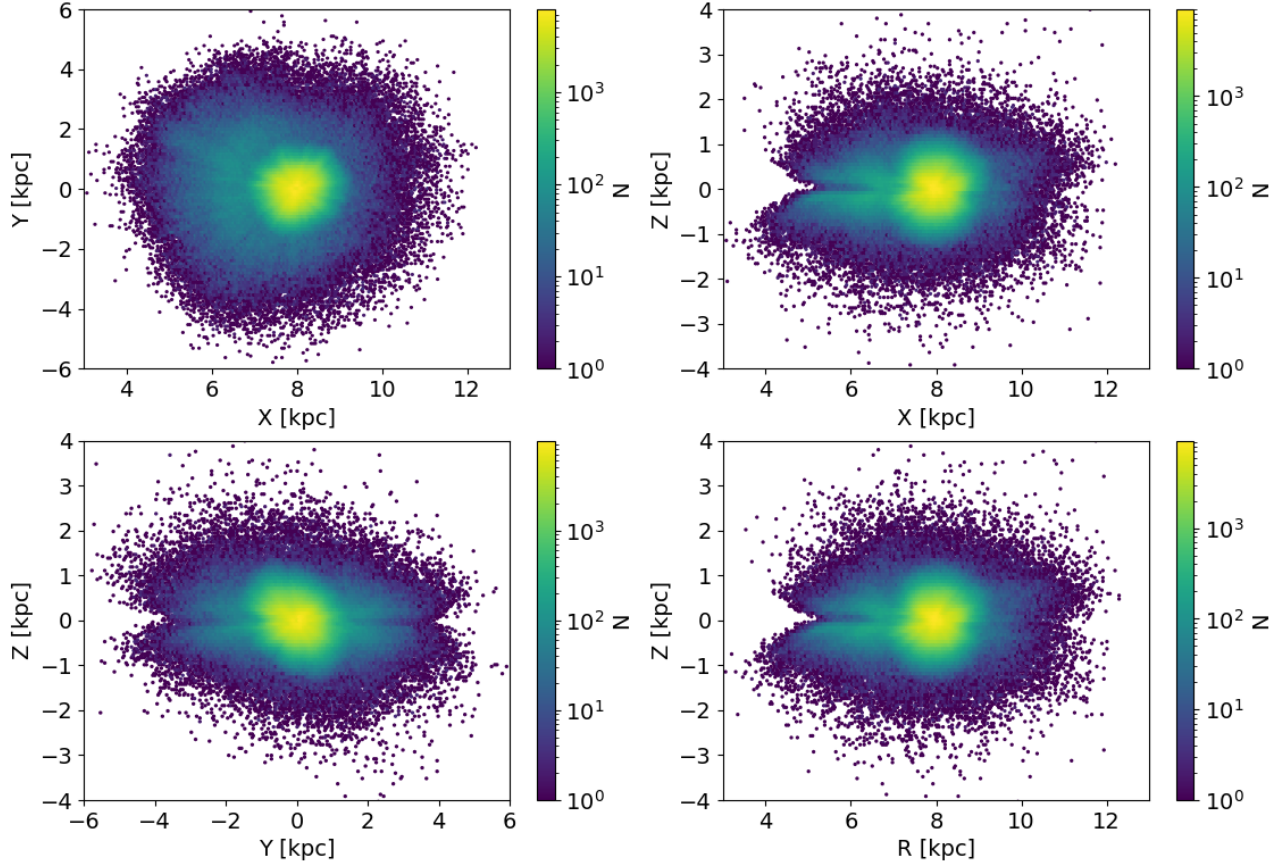


Figure 2. The distribution of stars shown in Figure 1 in the right-handed galactocentric Cartesian coordinates ($R_\odot = 8.0$ kpc). Note that the counts are shown on a log scale – the majority of stars are at distances below 1 kpc (the median distance is 620 pc).

luminosities, and their metallicities can be sufficiently accurately (0.1–0.2 dex) estimated from broad-band photometric data (Ivezić et al. 2008). They were principal stellar populations used for developing a stellar number density model in Jurić et al. (2008) and stellar kinematics models in Bond et al. (2010). While Gaia Data Release 3 data access tools could be used to construct an adequate sample of stars for comparison to SDSS results, an essentially perfect catalog for this purpose was recently published by the Gaia team.

Creevey, Sarro, Lobel et al. (Gaia Collaboration et al. 2023) constructed a carefully cleaned science-ready sample (“a golden sample of astrophysical parameters”) of F, G, K, and M stars listed in the Gaia Data Release 3 catalog. After quality cuts based on astrometric, photometric, and astrophysical parameters, along with other Gaia-based criteria, they provided a catalog of 3.3 million stars with measured and/or estimated astrophysical parameters using Gaia and other datasets (including effective temperature, metallicity, mass, age and spectral type). Of particular relevance to the analysis presented here, their FGKM sample included the following selection criteria: an effective signal-to-noise ratio cut applied through a limit on the $B_P - R_P$ color error $\sigma < 0.06$ mag, effective temperature $T_{eff} < 7500$ K, absolute magnitude in Gaia’s G band $M_G < 12$, and metallicity $[Fe/H] > -0.8$. Consequently, the sample is dominated by high-metallicity disk stars at distances of up to about 1 kpc (the median distance is 620 pc). In subsequent analysis, we use stellar distances computed by Bailer-Jones et al. (2021).

Figure 1 shows the distribution of this sample (hereafter the FGKM sample) in the Hertzsprung-Russell diagram, and also provides information about metallicity, interstellar dust reddening, and age distributions. Given distances, we computed galactocentric coordinates for all stars using eqs. 15–16 from Jurić et al. (2008). The spatial distribution of this sample is shown in Figure 2. For 1.73 million stars in this sample, radial velocities are also available. We

computed their velocities in the cylindrical coordinate system using eqs. 4–8 from Bond et al. (2010). These velocities, as well as proper motions for all the stars, are used for model validation in the next Section.

In addition to the FGKM sample, with a median distance of 620 pc, we also utilize another sample which allows us to extend our analysis to much more distant disk stars, as well as to low-metallicity halo stars. Andrae et al. (2023) published a catalog of over 17 million bright ($G < 16$) red giants, including estimates of their metallicity based on Gaia’s XP spectra. Figure 3 shows the rotational velocity vs. metallicity distribution for 2.5 million stars from the solar cylinder (galacto-centric cylindrical radius between 7 kpc and 10 kpc), as a function of distance from the Galactic plane. As evident, metallicity can be used to separate non-rotating low-metallicity halo stars from rotating high-metallicity disk stars. In the full red giants sample, there are 283,616 stars with $[\text{Fe}/\text{H}] < -1.2$, and of those 188,807 have good radial velocity measurements (that are not “NaN”). Hereafter, we refer to the latter sample as the “halo sample”; its spatial distribution in the Galaxy is shown in Figure 4.

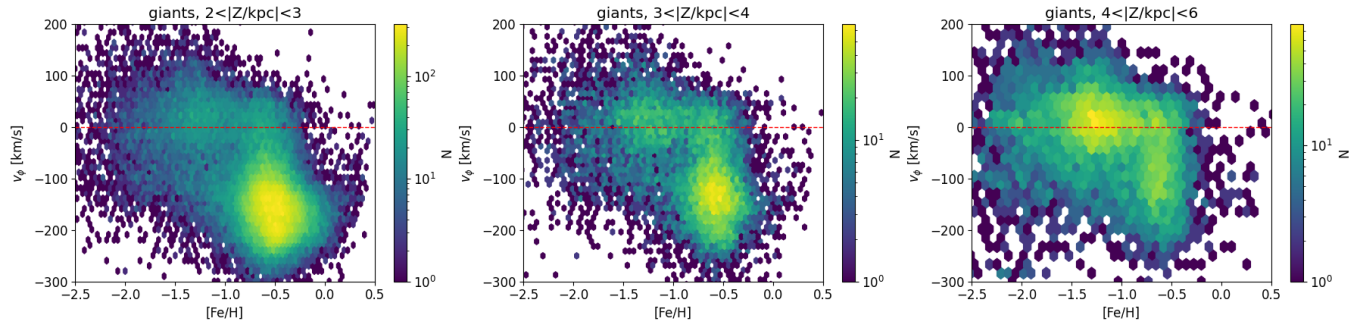


Figure 3. The rotational velocity vs. metallicity distribution of red giant stars from the Andrae et al. (2023) catalog that have a cylindrical galacto-centric radius between 7 kpc and 10 kpc, and for three bins of distance from the Galactic plane (left to right: 2–3 kpc, 3–4 kpc, 4–6 kpc). The mean rotational velocity for halo stars is consistent with 0, with metallicity $[\text{Fe}/\text{H}] < -1$, while for disk stars $[\text{Fe}/\text{H}] > -1$ and rotation slows down with distance from the plane.

2.1. Kinematic models derived from SDSS data

Bond et al. (2010) studied Milky Way kinematics using a sample of 18.8 million main-sequence stars with SDSS magnitude $14 < r < 20$ and proper-motion measurements derived from SDSS and POSS astrometry over a quarter of the sky at high Galactic latitudes ($|b| > 20^\circ$). Their sample also included $\sim 170,000$ stars with radial-velocity measurements from the SDSS spectroscopic survey. Distances to stars, in the range from 100 pc to 10 kpc, were determined using a color-based and metallicity-dependent photometric parallax relation (Jurić et al. 2008; Ivezić et al. 2008).

2.1.1. Kinematic model for disk stars

For disk stars, they found that in the region defined by $1 \text{ kpc} < |Z| < 5 \text{ kpc}$, where $|Z|$ is the distance from the Galactic plane, the rotational velocity for disk stars smoothly decreases, and all three components of the velocity dispersion increase, with $|Z|$. They developed a simple descriptive model for the overall kinematic behavior that captures these features over most of the probed volume, as follows.

The decrease of rotational velocity with $|Z|$ for disk stars (often referred to as asymmetric drift, velocity lag, or velocity shear; for more details and references to related work, see §3.4 in Ivezić et al. 2008) in the $|Z| = 1 – 4$ kpc range can be described by

$$\langle v_\phi \rangle = -205 + 19.2 \left| \frac{Z}{\text{kpc}} \right|^{1.25} \text{ km s}^{-1}. \quad (1)$$

The measured rotational velocity dispersion of disk stars increases with Z faster than can be attributed to measurement errors; their *intrinsic* velocity dispersion can be fit as

$$\sigma_\phi = 30 + 3.0 \left| \frac{Z}{\text{kpc}} \right|^{2.0} \text{ km s}^{-1}. \quad (2)$$

The errors on the power-law exponents of eqs. 1 and 2 are ~ 0.1 and ~ 0.2 , respectively.

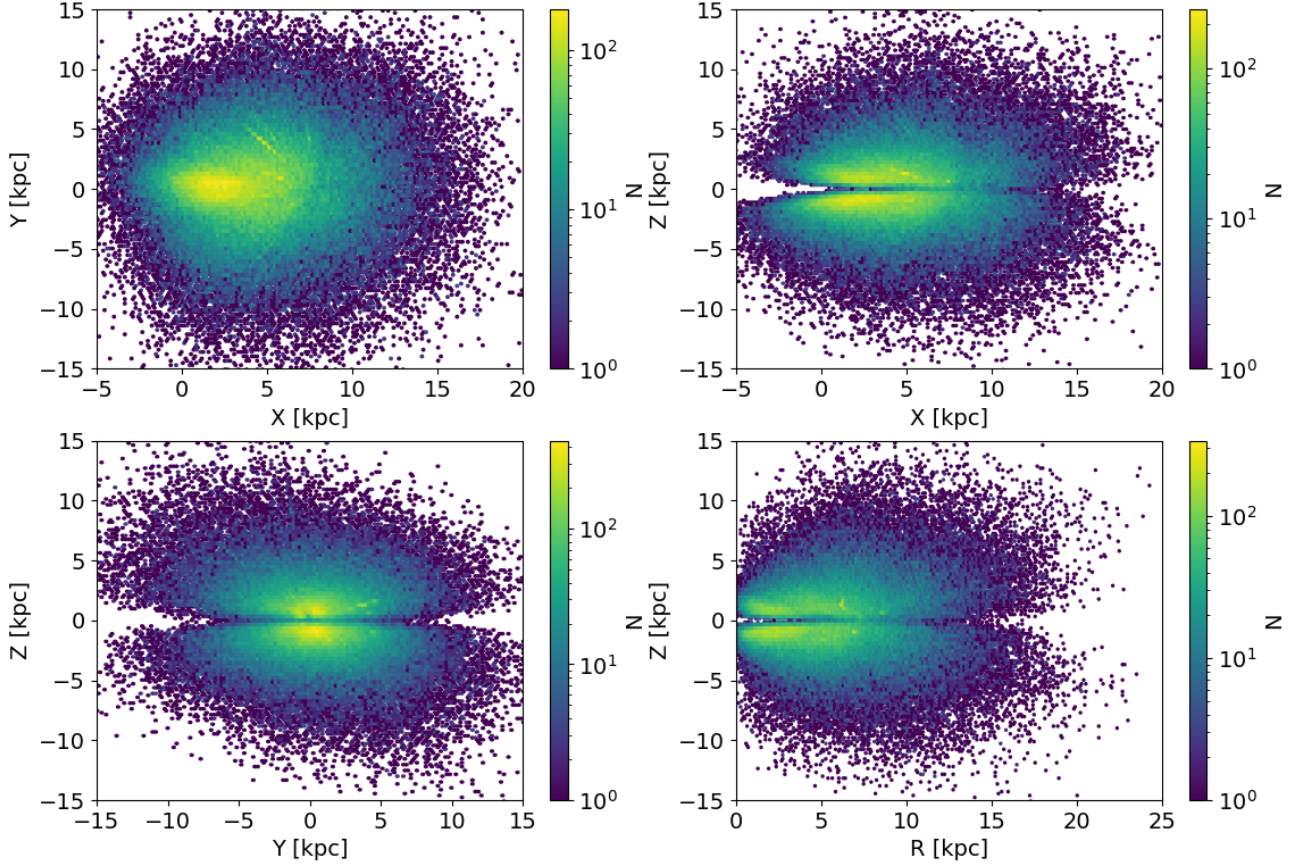


Figure 4. The distribution of 188,807 candidate halo red giant stars with $[\text{Fe}/\text{H}] < -1.2$. Their median distance is 6.0 kpc. Note significantly expanded axis limits compared to Figure 2.

However, it was also found that a description of the full velocity distribution based solely on the first and second moments (that is, by eqs. 1 and 2) does not fully capture the detailed data behavior. The observed non-Gaussian shape for the rotational (v_ϕ) component can be modeled by a sum of two Gaussians, with a fixed normalization ratio and a fixed offset of their mean values for $|Z| < 5$ kpc,

$$p(x = v_\phi | Z) = f_1 G[x | v_n(Z), \sigma_1] + f_2 G[x | v_n(Z) - \Delta v_n, \sigma_2], \quad (3)$$

where $G(x | \mu, \sigma)$ is Gaussian (normal) distribution, $f_1 = 0.75$, $f_2 = 0.25$, $\Delta v_n = 34 \text{ km s}^{-1}$, and velocity variation with $|Z|$ is captured by

$$v_n(Z) = v_0 + 19.2 \left| \frac{Z}{\text{kpc}} \right|^{1.25} \text{ km s}^{-1}, \quad (4)$$

with $v_0 = -194 \text{ km s}^{-1}$. The intrinsic velocity dispersions, σ_1 and σ_2 , increase with $|Z|$ and are modeled as $a + b|Z|^c$, with the best-fit parameters a , b and c listed in Table 1 from Bond et al. (2010) ($c = 2.0$ for both).

The mean values for the v_R and v_Z components were found to be zero, as expected. Their intrinsic dispersions for disk stars vary with Z and are described by the following expressions:

$$\sigma_R = 40 + 5.0 \left| \frac{Z}{\text{kpc}} \right|^{1.5} \text{ km s}^{-1}. \quad (5)$$

and

$$\sigma_Z = 25 + 4.0 \left| \frac{Z}{\text{kpc}} \right|^{1.5} \text{ km s}^{-1}. \quad (6)$$

They also found that the σ_R/σ_ϕ ratio for disk stars has a constant value of ~ 1.35 for $Z < 1.5$ kpc, and decreases steadily at larger Z to about 1 at $Z \sim 4$ kpc.

We note that for stars in the analyzed FGKM sample, the mean age increases and the mean metallicity decreases with the distance from the Galactic plane, with the latter also observed in analyzed SDSS data. For attempts to interpret these correlations using a radial migration model for disk stars, see [Loebman et al. \(2011\)](#).

In the next Section, we compare these models to Gaia measurements for stars in the FGKM and red giant samples. In particular, we aim to test whether the above fits to the median rotational velocity and velocity dispersion, constrained by luminous blue stars with $r > 14$ used in the SDSS study, can be successfully extrapolated closer to the Galactic plane, as probed by Gaia measurements for stars with $r < 14$ in the FGKM sample.

2.1.2. Kinematic model for halo stars

Bond et al. found that kinematics of halo stars in their sample, that was confined to galacto-centric radial distances in the range 5–20 kpc, admit an exceedingly simple model description. Their dataset was fully explained with no net rotation and a model triaxial velocity ellipsoid that is invariant in spherical coordinates, with the following velocity dispersions: $\sigma_r = 141$ km s $^{-1}$, $\sigma_\phi = 85$ km s $^{-1}$, and $\sigma_\theta = 75$ km s $^{-1}$, with uncertainties of about 5–10 km s $^{-1}$. This remarkable alignment of the halo velocity ellipsoid with spherical coordinates (halo stars “know” where the Galactic center is) represents a strong constraint on the shape of gravitational potential—the potential must be close to spherically symmetric at least within about 20 kpc from the Galactic center (for more details and references, see [Loebman et al. 2014; Everall et al. 2019](#)).

3. RESULTS

Here we test the validity of the Bond et al. kinematic models for disk and halo stars, as enabled by the high-metallicity FGKM sample and the red giant sample introduced in the preceding Section. We first discuss the behavior of the first two statistical moments (mean and dispersion) for 3-dimensional velocity distribution and then compare the predicted and observed shapes of the rotational velocity distribution in more detail. We test model predictions for the behavior of quantities directly measured by Gaia, stellar radial velocities and proper motions, across the whole sky. Finally, we verify that the behavior of Gaia data for halo stars is consistent with a velocity ellipsoid that is spatially invariant when expressed in spherical coordinates.

3.1. Comparison of predicted and observed 3-dimensional velocity distribution for disk stars

We first emulate the top left panels in Figures 5, 7 and 11 from the Bond et al. study. We select stars towards the North and South Galactic poles ($|b| > 80^\circ$) and show the variation of their velocity components with $|Z|$ in [Figure 5](#). Due to the galactic latitude constraint, the v_Z component is dominated by the radial velocity measurements while the other two components are dominated by proper motion measurements. Compared to the Bond et al. high-luminosity sample, the distance range probed by Gaia’s FGKM sample is closer: from about 50 pc to about 1 kpc vs. 0.8–5 kpc (at the far end, the SDSS sample is limited by sample contamination due to halo stars).

The Bond et al. model predictions for the velocity mean and dispersion are in agreement with Gaia’s observations. In particular, the gradient of the rotational velocity with $|Z|$ is evident, and the extrapolation of SDSS rotational velocity measurements to $Z = 0$ is quantitatively supported by Gaia. The same conclusions remain valid when the full sample is considered (that is, without the $|b| > 80^\circ$ restriction).

The < 1 kpc distance range probed by FGKM stars is significantly extended with the red giant sample, as illustrated in [Figure 6](#). In conclusion, the Bond et al. models for the velocity mean and dispersion of disk stars appear validated in the $|Z|$ range 0–5 kpc, without any appreciable north-south asymmetry.

3.2. Comparison of predicted and observed shapes of the rotational velocity distribution for disk stars

As already suggested in [Ivezić et al. \(2008\)](#) and confirmed by Bond et al. (see their Figure 6), the shape of the rotational velocity distribution for disk stars is strongly non-Gaussian (skewed) and it evolves with the distance from the Galactic plane. Histograms based on Gaia’s data shown in [Figure 7](#) confirm this expectation. Furthermore, new data still admit detailed quantitative modeling of observed distributions as a sum of two Gaussians, with a fixed normalization ratio and a fixed offset of their mean values (see [eq. 3](#)). Since Gaia’s velocity measurement errors are negligible in this context (compared to the much larger width of the observed velocity distributions; for validation

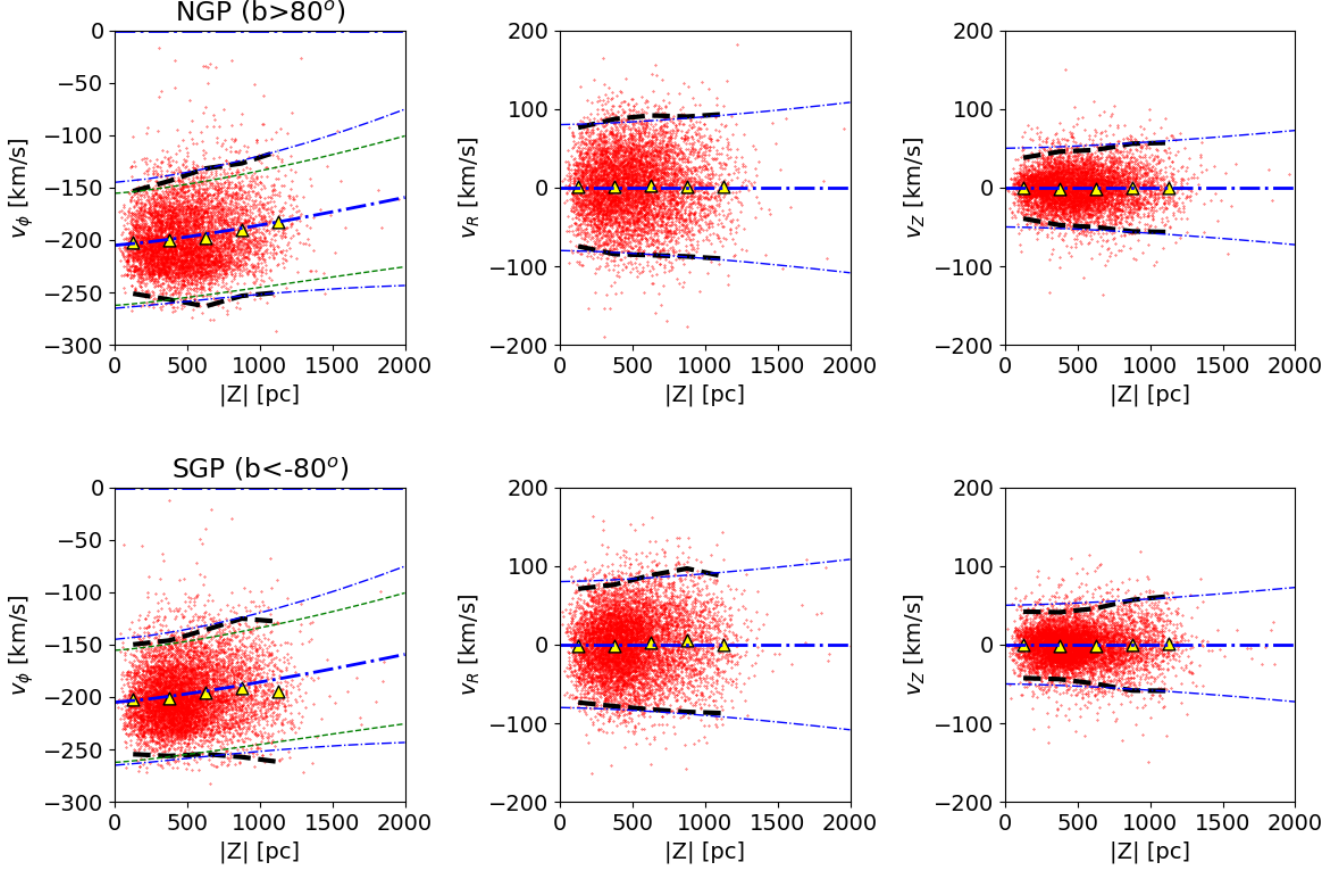


Figure 5. The variation of cylindrical velocity components with distance from the plane, $|Z|$, for FGKM stars with measured radial velocities, shown as dots. The top row shows 6,548 stars towards the North Galactic Pole ($b > 80^\circ$) and the bottom row shows 7,578 stars towards the South Galactic Pole ($b < -80^\circ$). Triangles show the mean values in bins of $|Z|$ and the thick dashed lines show the $\pm 2\sigma$ envelope around means, where σ is the standard deviation for each bin (i.e., velocity dispersion). The thick dot-dashed lines are models for the mean velocity (0 for v_R and v_Z , and given by eq. 1 for v_ϕ). The thin dot-dashed lines show the $\pm 2\sigma$ envelope, with σ (velocity dispersion) given by eqs. 2, 5, and 6, for ϕ , R and Z panels, respectively. The thin dashed lines in the two left panels also show $\pm 2\sigma$ envelopes, but with the velocity dispersion computed using eq. 3 (see § 3.2).

using quasar data, see Appendix), we have reoptimized fits by allowing six parameters to vary. Their best-fit values remain close to the SDSS values: $f_1 = 0.40$, $f_2 = 0.60$, $v_0 = -186 \text{ km s}^{-1}$, $\Delta v_n = 38 \text{ km s}^{-1}$, $a_1 = 22 \text{ km s}^{-1}$ and $a_2 = 17 \text{ km s}^{-1}$.

When the resulting re-optimized pdf, $p(x = v_\phi | Z)$, is used to evaluate the mean $\langle v_\phi \rangle$ and its dispersion σ_ϕ as functions of Z , there is no discernible change for the former compared to eq. 1, while the latter is about 20% smaller than values given by eq. 2 (for illustration of the difference, see the two left panels in Figure 5). Since there is no implied physics in this two-component statistical model of the skewed velocity distribution, minor numerical adjustments of the few free model parameters are probably inconsequential.

These conclusions based on the FGKM sample are supported by the behavior of the red giant sample, as illustrated in Figure 8. In particular, the vertical gradient of rotational velocity is evident.

3.3. Comparison of predicted and observed radial velocity and proper motion sky distributions for disk stars

As the final test, we extrapolate the Bond et al. model from the quarter of the sky observed by SDSS and compare its predictions for the variation of mean proper motions and radial velocities to Gaia’s measurements across the whole sky. The three left panels in Figure 9 show mean proper motion components per pixel and mean radial velocity per pixel for stars with distances in the range 400 pc to 600 pc. Their strong variation across the sky is evident and is

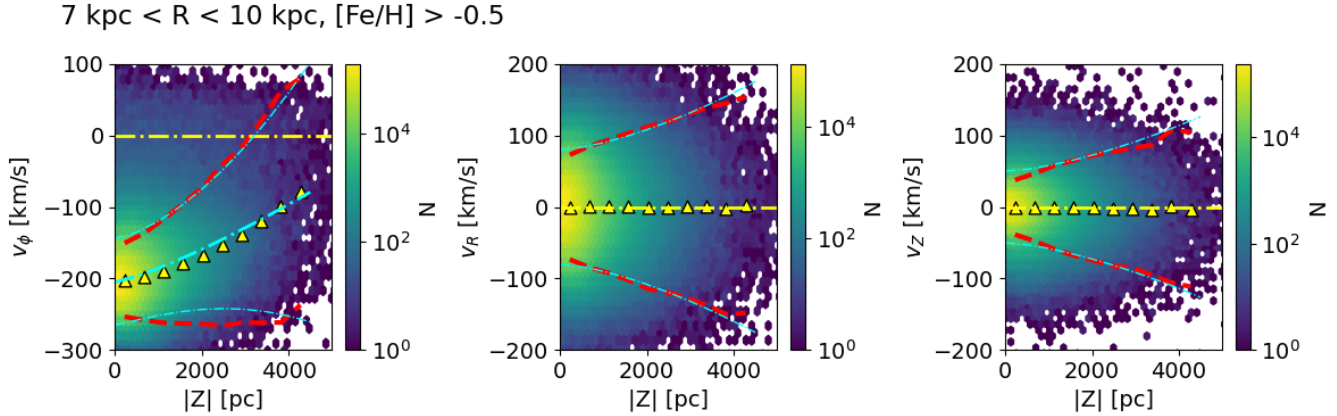


Figure 6. Similar to Figure 5, except that here about five times larger distances are probed with 4.3 million red giant stars that have $[\text{Fe}/\text{H}] > -0.5$ and cylindrical galacto-centric radius between 7 kpc and 10 kpc. The meaning of symbols and lines is the same as in Figure 5, and exactly the same models are shown.

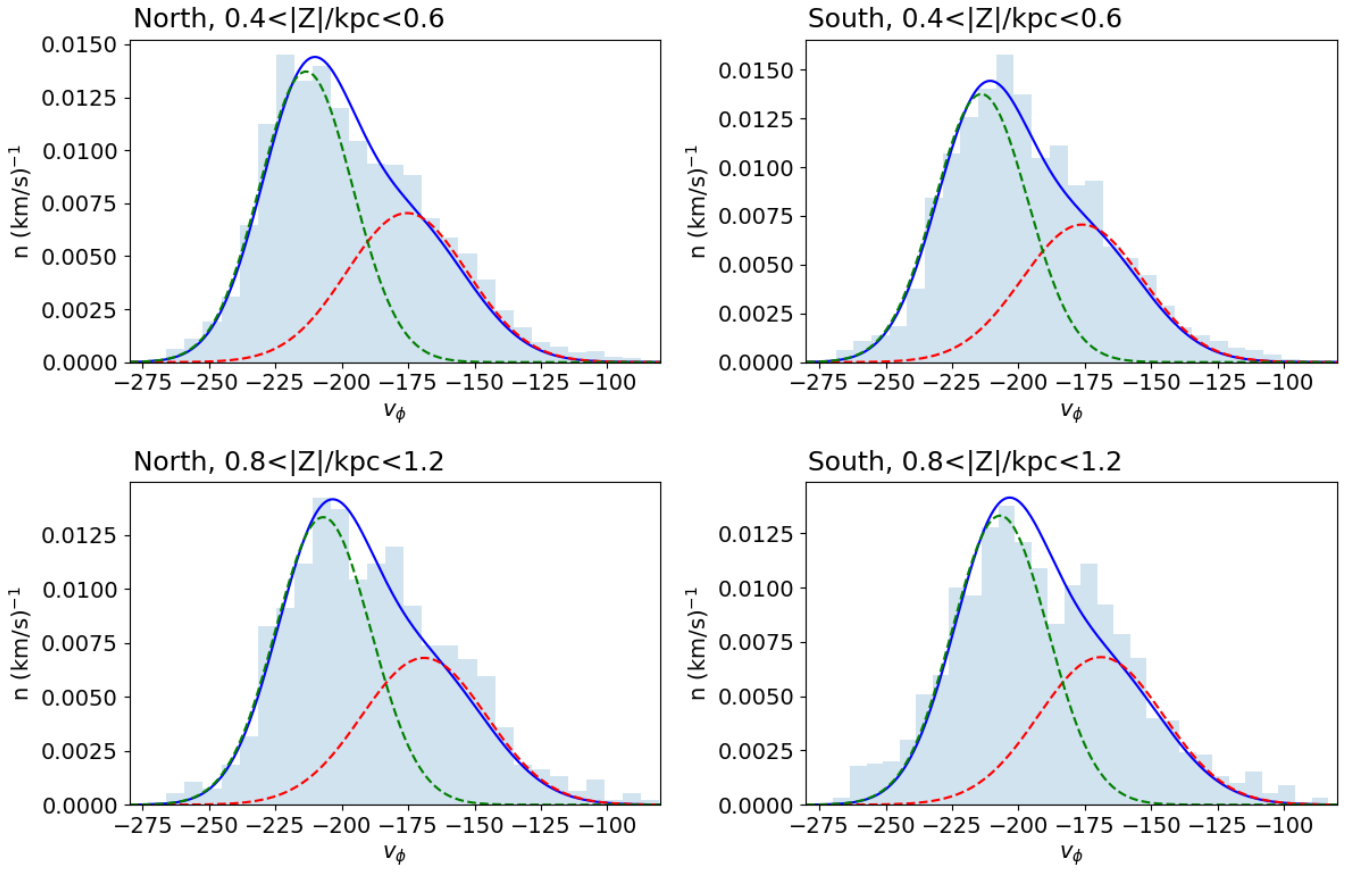


Figure 7. A comparison of the observed rotational velocity distribution (v_ϕ) for FGKM stars, shown as histograms, and a two-component model (dashed lines: individual components; solid line: their sum) given by eq. 3 (using updated parameters discussed in text; the same Z -dependent model is shown in all four panels). The four panels show results for two $|Z|$ bins (top row vs. bottom row) and towards North and South ($|b| > 80^\circ$, left vs. right). The sample sizes are about 4,000 stars for the nearer $|Z|$ bin and about 900 stars for the more distant bin.

mostly due to projection effects of the solar motion (and a little bit due to spatial variation of the rotational velocity

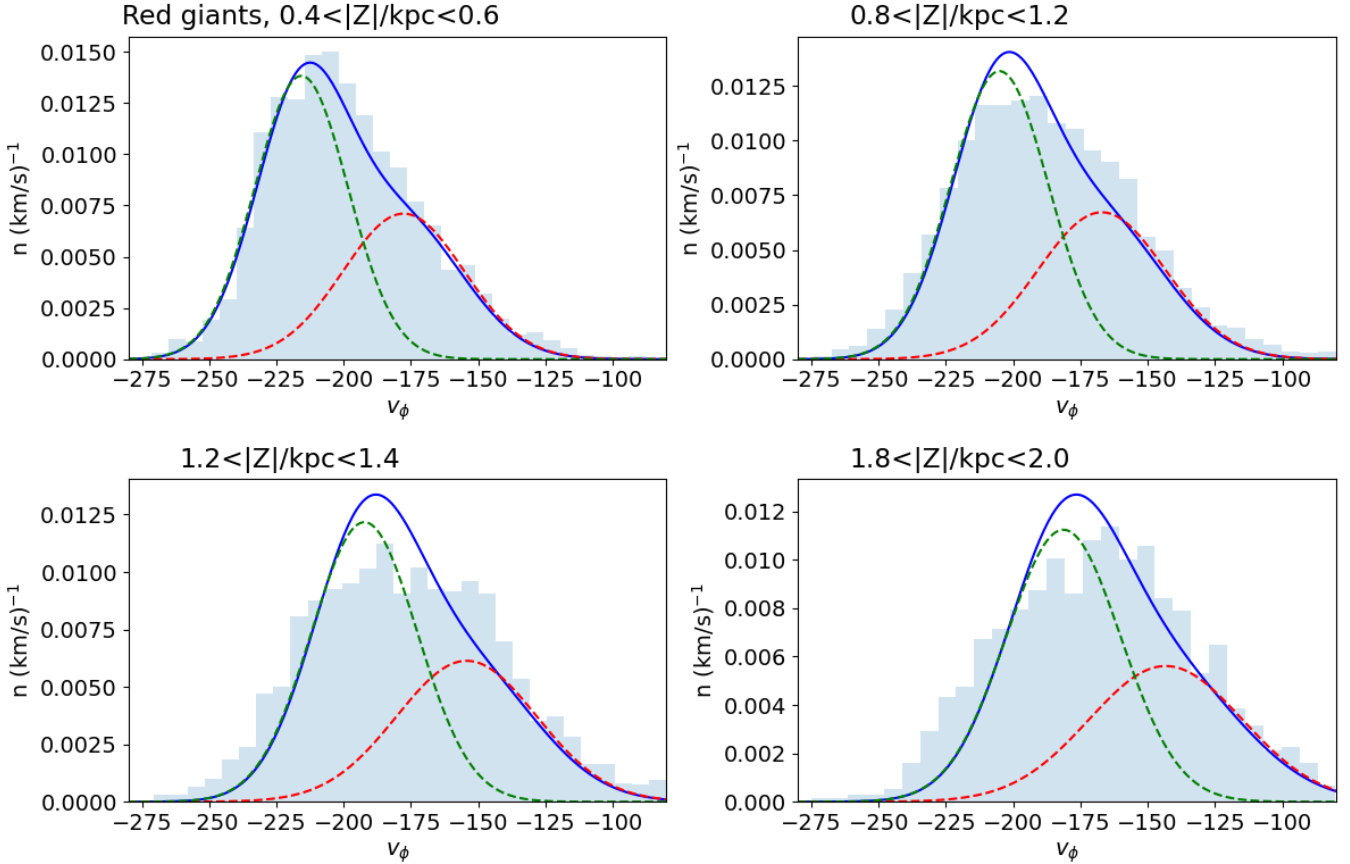


Figure 8. Analogous to Figure 7, except for a subsample of the red giant sample shown in Figure 6 restricted to $|b| > 60^\circ$. The top two panels show the same $|Z|$ bins as in Figure 7, while the two bottom panels extend to larger $|Z|$. The sample sizes vary from 10,000 stars to 2,000 stars for the most distant bin.

component with $|Z|$). The panels on the right show residuals after subtracting proper motion and radial velocity values predicted by the Bond et al. model described in § 2.1. As evident, the model fully captures the observed behavior. The only potentially significant feature is observed for radial velocity residuals towards the Galactic center, at about $0 < b < 30^\circ$. This region was not observed by SDSS and we are not aware of any kinematic or other stellar features reported for that region (e.g., the famous Sgr dwarf galaxy is located at negative galactic latitudes). A possibility that these residuals reflect faulty measurements could be, at least in principle, easily checked because most of these stars are relatively bright ($r \sim 14$).

We note that the data maps for stars with distances in the range of 800 pc to 1.2 kpc look qualitatively the same, except that the magnitude of proper motion is smaller by about a factor of two, as expected. The maps of residuals appear the same, except for the radial velocity residual “feature”, which is observed at about 15 degrees higher latitudes than for the first distance bin.

The red giant sample can be used to extend this comparison to distances where the rotational velocity component is much smaller than locally. We first established that the behavior for red giants in the 0.4–0.6 kpc distance bin is essentially identical as shown for the FGKM sample in Figure 9. The corresponding plot for red giants in the 2.8–3.2 kpc distance bin is shown in Figure 10. Due to about six times larger distances, the morphology of data panels is rather different from that in Figure 9 (especially for radial velocity, where projection effects of rotational velocity component dominate). Nevertheless, the model for disk kinematics described in § 2.1 fully captures the data behavior, as shown by vanishing maps of (data-model) residuals.

3.4. Comparison of predicted and observed 3-dimensional velocity distribution for halo stars

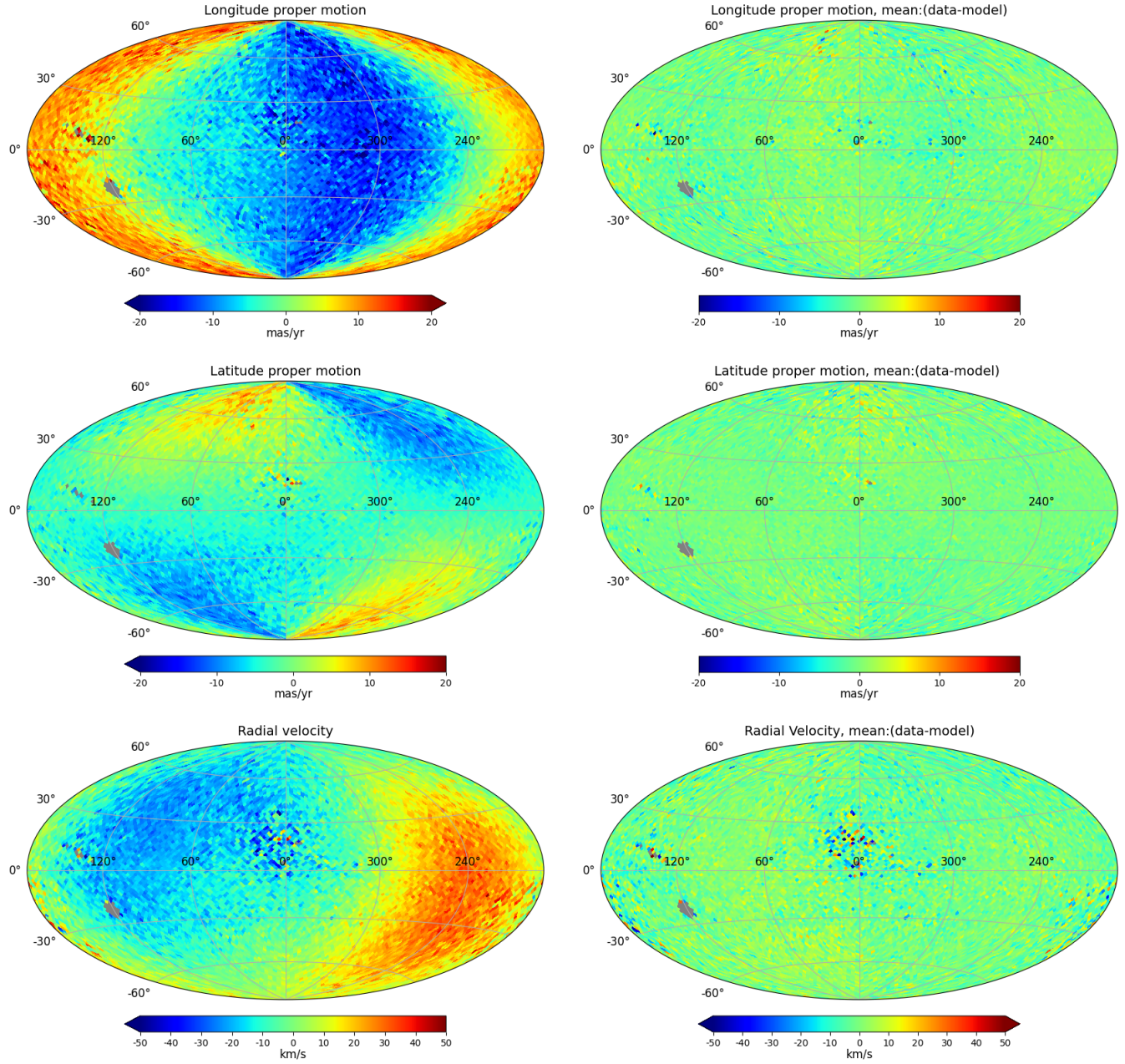


Figure 9. The top two left panels show observed distributions of mean proper motion per pixel (top: longitude; middle: latitude) for 868,859 stars in the 0.4–0.6 kpc distance bin. The bottom left panel shows the observed distribution of mean radial velocity for a subsample of 400,782 stars with good measurements. The healpix $n_{\text{side}}=32$ maps are shown in the Hammer projection of galactic coordinates. The maps on the right show residuals (using the same color-coding scale) after subtracting model values computed using eq. 1 for v_ϕ and with $\langle v_R \rangle = \langle v_Z \rangle = 0$.

Bond et al. found that the kinematics of halo stars can be modeled with a triaxial velocity ellipsoid that is invariant in spherical coordinates. Motivated by this finding, we show in Figure 11 three spherical velocity components for halo red giants as functions of distance from the Galactic plane. Unlike the strong dependence on the velocity dispersion on $|Z|$ for disk stars seen in Figures 5 and 6, velocity dispersion for halo stars as measured by Gaia is spatially invariant, confirming earlier results by Bond et al. We note that small deviation of mean rotational velocity from zero at $|Z| < 1$ kpc seen in the left panel is probably due to sample contamination by much more numerous disk stars (at $|Z| = 0$, halo stars contribute only about 0.5% of the total count, see Table 10 in Jurić et al. 2008).

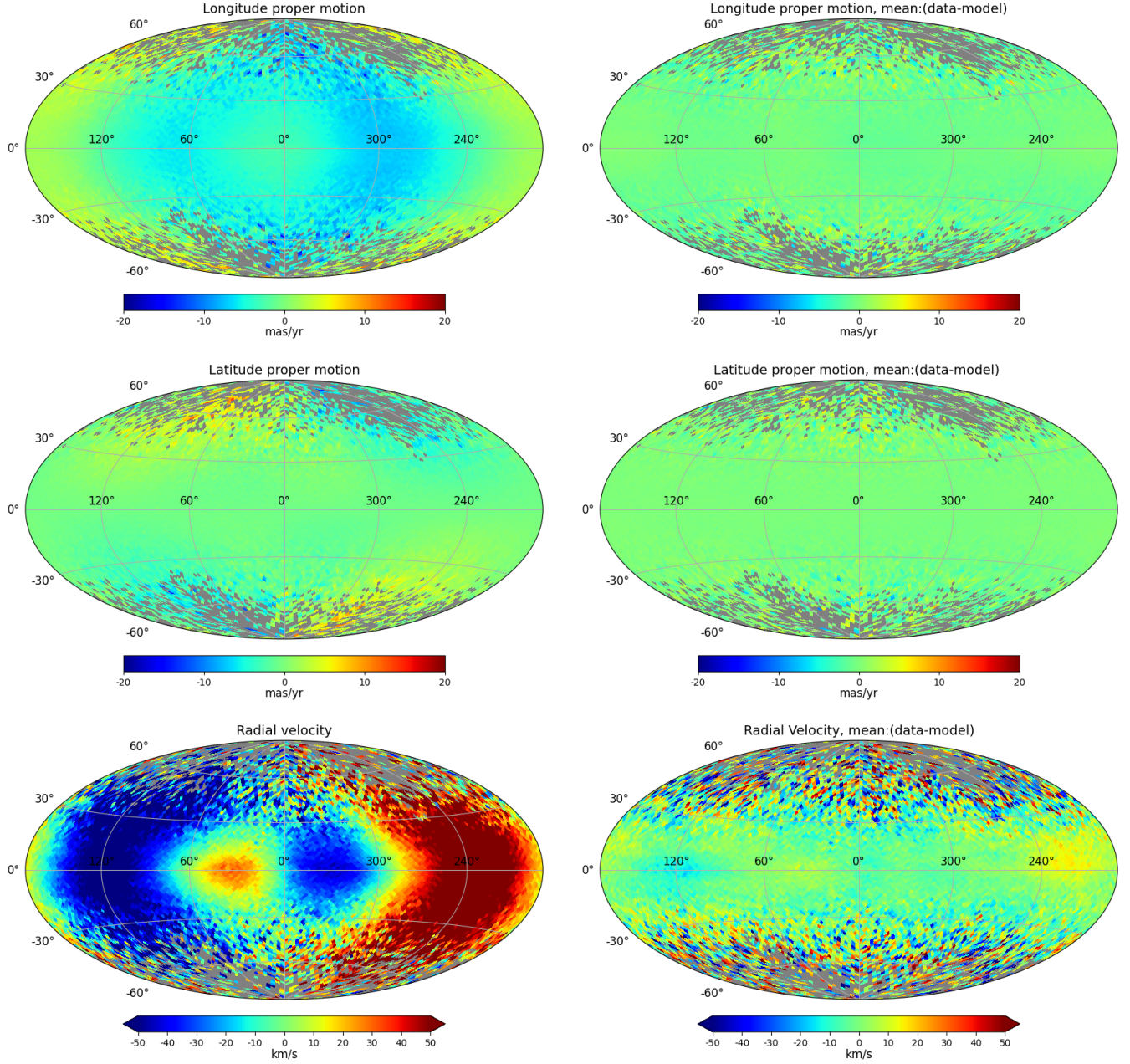


Figure 10. Analogous to Figure 9, except for a sample of 1.05 million red giants with $[\text{Fe}/\text{H}] > -0.5$ in the 2.8–3.2 kpc distance bin. Note that observed proper motions are much smaller due to about six times larger distances, while radial velocity variation with galactic longitude is much stronger due to the projection effects of the rotational velocity component.

Gaia data analyzed here provide strong support for a halo velocity ellipsoid that is invariant in spherical coordinates. When the velocity ellipsoid is expressed in cylindrical coordinates instead, a strong covariance is seen between the v_Z and v_R components. We illustrate this covariance in Figure 12. The observed tilt varies with position such that the velocity ellipsoid points towards the Galactic center (see also [Everall et al. 2019](#)).

4. DISCUSSION AND CONCLUSIONS

We validated the [Bond et al. \(2010\)](#) kinematic models for the Milky Way’s disk and halo stars with Gaia Data Release 3 data.

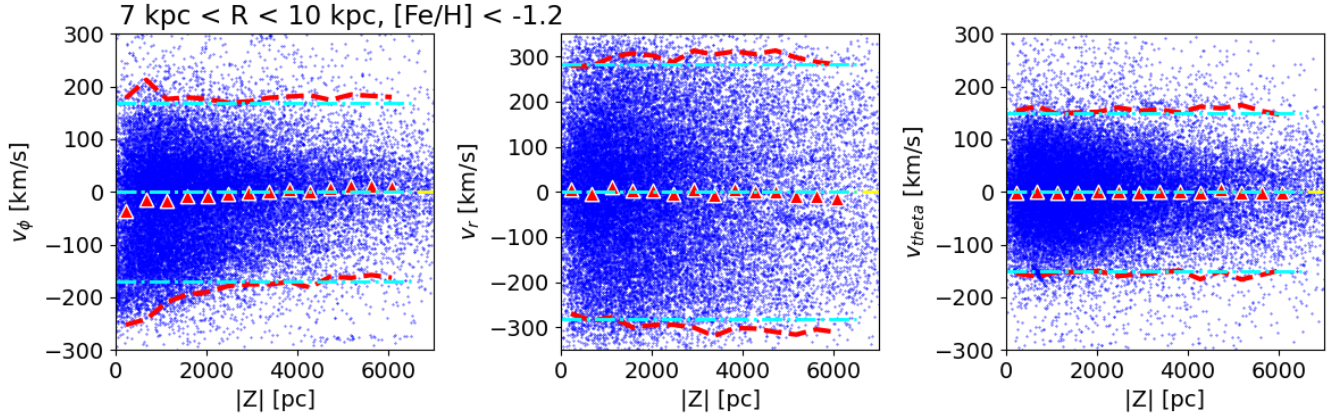


Figure 11. The variation of spherical velocity components with distance from the plane, $|Z|$, for $\sim 34,000$ candidate halo red giants from the solar cylinder with measured radial velocities and $[\text{Fe}/\text{H}] < -1.2$. Triangles show the mean values in bins of $|Z|$ and the thick dashed lines show the $\pm 2\sigma$ envelope around means, where σ is standard deviation for each bin (i.e., velocity dispersion). The dot-dashed lines represent the halo velocity ellipsoid model described in Section 2.1.2.

For disk stars, the gradient of rotational velocity with $|Z|$ is evident in Gaia’s data, and the extrapolation of SDSS rotational velocity measurements to $Z = 0$ is also supported by Gaia. The models for the velocity mean and dispersion are validated in the $|Z|$ range 0–5 kpc, without appreciable north-south asymmetry.

We note that the v_ϕ vs. v_R distribution close to the Galactic plane (closer than a few hundred pc) is very complex and cannot be described by a standard Schwarzschild ellipsoid (for details and references, see §3.1 in Ivezić et al. 2008). The panels in Figure 13 are analogous to Figure 4 from Bond et al. (2010). The so-called “Eggen’s moving groups” (Eggen 1996) are clearly visible at distances smaller than 300 pc and cannot be described in detail by the models discussed here.

The all-sky proper motion and radial velocity test based on the FGKM sample discussed in §3.3 is encouraging but we caution that that most of the observed variation of measured quantities across the sky is due to projection effects of the solar motion; the spatial variation of the rotational velocity component with $|Z|$ is only a minor contribution. Therefore, the main implication of that test is that the FGKM sample supports our adopted solar motion values taken from Dehnen & Binney (1998), which were derived using HIPPARCOS data. The test based on red giants is stronger because it reaches to about six times larger distances.

For halo stars, the spatial invariance of their velocity ellipsoid when expressed in spherical coordinates is also confirmed by Gaia data at galacto-centric radial distances of up to 15 kpc. For related work, please see Everall et al. (2019).

Given these successful tests, the Bond et al. kinematic models for disk and halo stars are adequate for implementation in simulated catalogs of Milky Way’s stellar content, such as the recent TRILEGAL-based simulated LSST catalog by Dal Tio et al. (2022). We note that, as discussed by Ivezić et al. (2012) and Ivezić et al. (2019), LSST will provide its own kinematic constraints with numerous main-sequence stars out to distances of about 30 kpc, significantly further than possible with Gaia data (due to several magnitudes fainter survey limit).

DATA AVAILABILITY

All the code required to reproduce our results, along with the dataset, has been made available online on GitHub.³

ACKNOWLEDGMENTS

We are thankful to the 2023 Vatican Observatory Summer School in Observational Astronomy and Astrophysics, where this work originated. S.C. acknowledges funding provided by the University of Delaware through the Graduate Student Travel Award. Ž.I. acknowledges funding by the Fulbright Foundation and thanks the Ruđer Bošković Institute for hospitality.

³ <https://github.com/sidchaini/MWKinematicsFGKM>

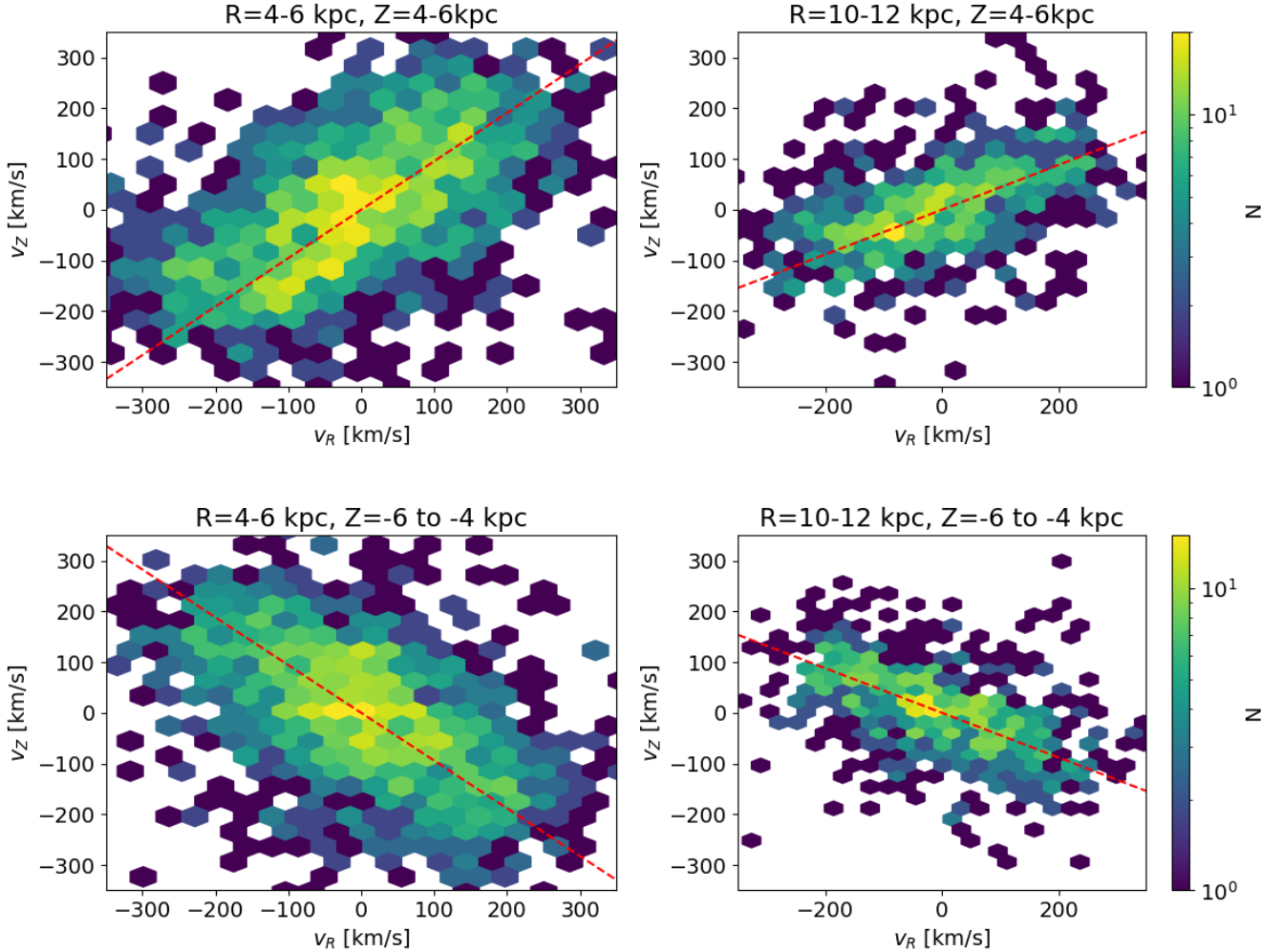


Figure 12. Illustration of the change of orientation of velocity ellipsoid in cylindrical coordinates for halo stars, selected to have $[\text{Fe}/\text{H}] < -1.2$ and selected from a narrow range of cylindrical coordinates, as shown above each panel. The number of stars is about 1,600 for bins with smaller R (left) and 800 for bins on the right. The top row shows bins above the plane and the bottom row their symmetric counterparts below the plane (the Sun’s position is in the middle of the figure). The dashed lines mark the direction towards the Galactic center. The change of the velocity ellipsoid tilt in cylindrical coordinates is evident; however, the velocity ellipsoid in spherical coordinates is invariant throughout the probed volume, as illustrated by these four spatial bins.

Funding for the SDSS and SDSS-II has been provided by the Alfred P. Sloan Foundation, the Participating Institutions, the National Science Foundation, the U.S. Department of Energy, the National Aeronautics and Space Administration, the Japanese Monbukagakusho, the Max Planck Society, and the Higher Education Funding Council for England. The SDSS Web Site is <https://www.sdss.org/>.

This work has made use of data from the European Space Agency (ESA) mission Gaia <https://www.cosmos.esa.int/gaia>, processed by the Gaia Data Processing and Analysis Consortium (DPAC, <https://www.cosmos.esa.int/web/gaia/dpac/consortium>). Funding for the DPAC has been provided by national institutions, in particular, the institutions participating in the Gaia Multilateral Agreement.

Facilities: Sloan Digital Sky Survey, Gaia

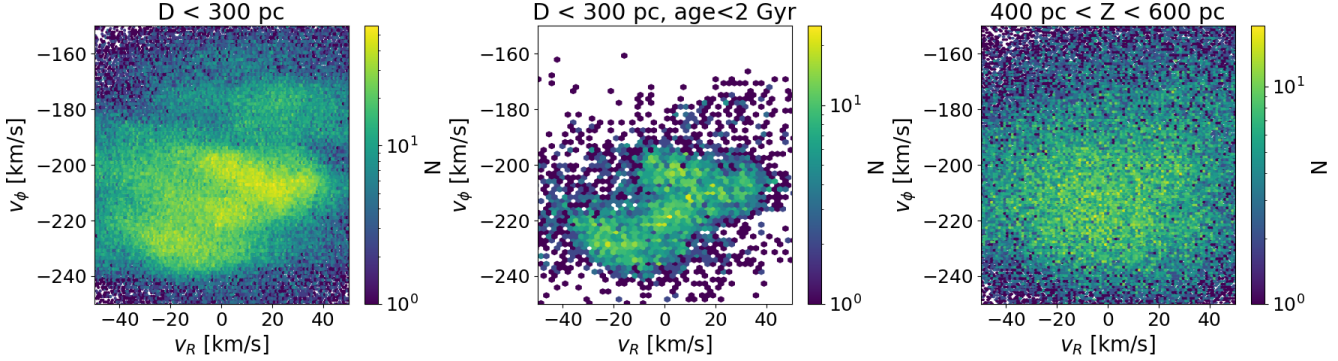


Figure 13. A comparison of distributions in the v_ϕ vs. v_R diagram for three different samples of disk stars: a nearby sample of 276,453 stars at distances below 300 pc (left), its subsample consisting of 6,108 stars younger than 2 Gyr (middle), and a sample of 237,660 stars at distances from the Galactic plane in the range of 400–600 pc. Complex structure, known in the literature as “Eggen’s moving groups”, is evident at distances below 300 pc. For example, the feature at $(v_R = -25, v_\phi = -230)$ corresponds to the Sirius moving group, the feature at $(v_R = 0, v_\phi = -220)$ is the Coma B moving group, the feature at $(v_R = 0, v_\phi = -200)$ is the Pleiades moving group, and the Hyades moving group is seen at $(v_R = 30, v_\phi = -210)$.

Software: numpy (Oliphant 2006), matplotlib (Hunter 2007), seaborn (Waskom 2021), scipy (Jones et al. 2001–), pandas McKinney (2010), astropy (Astropy Collaboration et al. 2013, 2018), astroML (VanderPlas et al. 2012), Jupyter (Kluyver et al. 2016), Python (Van Rossum & Drake 2009).

APPENDIX

Validation of proper motion systematic and random uncertainties using quasars

We tested Gaia’s proper motions and their uncertainties using spectroscopically confirmed quasars from SDSS Data Release 7. There are $\sim 367,000$ SDSS quasars with Gaia’s non-negative proper motion errors. Their median proper motion per coordinate is about 0.01 mas/yr (indicating no substantial systematic measurement errors) and the median proper motion magnitude is about 1.1 mas/yr (indicating typical measurement uncertainty; the median magnitude of this sample is $G \sim 20$; for the FGKM sample analyzed here, with $G < 18$, the proper motion uncertainties are < 0.15 mas/yr).

We have verified that the width of proper motion per coordinate normalized by reported uncertainties (i.e. the width of corresponding χ distributions) is 1.07 and 1.09, demonstrating Gaia’s reliable estimates of measurement uncertainties.

We didn’t find any significant variation of the median quasar proper motion per coordinate with position on the sky. The only “interesting feature” in the data is increased scatter of proper motion per coordinate measurements in the so-called SDSS Stripe 82 region by about 50% compared to the rest of SDSS sky. This effect is easily understood as due to deeper quasar sample in that region (due to details in SDSS spectroscopic target selection) and the increase of Gaia’s measurement uncertainties with magnitude (and verified through no substantial increase in the corresponding χ distributions).

REFERENCES

- Andrae, R., Rix, H.-W., & Chandra, V. 2023, ApJS, 267, 8
 Astropy Collaboration, Robitaille, T. P., Tollerud, E. J., et al. 2013, A&A, 558, A33
 Astropy Collaboration, Price-Whelan, A. M., Sipőcz, B. M., et al. 2018, AJ, 156, 123
 Bailer-Jones, C. A. L., Rybizki, J., Fouesneau, M., Demleitner, M., & Andrae, R. 2021, AJ, 161, 147
 Bond, N. A., Ivezić, Ž., Sesar, B., et al. 2010, ApJ, 716, 1
 Dal Tio, P., Pastorelli, G., Mazzi, A., et al. 2022, ApJS, 262, 22
 Dehnen, W., & Binney, J. J. 1998, MNRAS, 298, 387

- Eggen, O. J. 1996, AJ, 112, 1595
- Everall, A., Evans, N. W., Belokurov, V., & Schönrich, R. 2019, MNRAS, 489, 910
- Gaia Collaboration, Brown, A. G. A., Vallenari, A., et al. 2021, A&A, 649, A1
- Gaia Collaboration, Creevey, O. L., Sarro, L. M., et al. 2023, A&A, 674, A39
- Hunter, J. D. 2007, Computing In Science & Engineering, 9, 90
- Ivezić, Ž., Beers, T. C., & Jurić, M. 2012, ARA&A, 50, 251
- Ivezić, Ž., Sesar, B., Jurić, M., et al. 2008, ApJ, 684, 287
- Ivezić, Ž., Kahn, S. M., Tyson, J. A., et al. 2019, ApJ, 873, 111
- Jones, E., Oliphant, T., Peterson, P., et al. 2001–, SciPy: Open source scientific tools for Python, , , [Online; accessed 1 today]
- Jurić, M., Ivezić, Ž., Brooks, A., et al. 2008, ApJ, 673, 864
- Kluyver, T., Ragan-Kelley, B., Pérez, F., et al. 2016, in Positioning and Power in Academic Publishing: Players, Agents and Agendas, ed. F. Loizides & B. Schmidt, IOS Press, 87 – 90
- Loebman, S. R., Ivezić, Ž., Quinn, T. R., et al. 2012, ApJL, 758, L23
- Loebman, S. R., Roškar, R., Debattista, V. P., et al. 2011, ApJ, 737, 8
- Loebman, S. R., Ivezić, Ž., Quinn, T. R., et al. 2014, ApJ, 794, 151
- McKinney, W. 2010, in Proceedings of the 9th Python in Science Conference, ed. S. van der Walt & J. Millman, 51 – 56
- Oliphant, T. E. 2006, A guide to NumPy, Vol. 1 (Trelgol Publishing USA)
- Van Rossum, G., & Drake, F. L. 2009, Python 3 Reference Manual (Scotts Valley, CA: CreateSpace)
- VanderPlas, J., Connolly, A. J., Ivezić, Ž., & Gray, A. 2012, in Proceedings of Conference on Intelligent Data Understanding (CIDU), pp. 47–54, 2012., 47–54
- Waskom, M. L. 2021, Journal of Open Source Software, 6, 3021